Separation and Purification Technology 116 (2013) 319–326

Contents lists available at SciVerse ScienceDirect

Separation and Purification Technology

journal homepage: www.elsevier.com/locate/seppur

Parameter estimation and rate model simulation of partial breakthrough of bovine serum albumin on a column packed with large Q Sepharose anion-exchange particles

Tingyue Gu [a,*], Ganesh Iyer [b], Kwok-Shun C. Cheng [b]

[a] Department of Chemical and Biomolecular Engineering, Ohio University, Athens, OH 45701, United States
[b] BioProcess R&D, Millipore Corporation, 80 Ashby Road, M1 North, Bedford, MA 01730, United States

ARTICLE INFO

Article history:
Received 27 February 2013
Received in revised form 29 April 2013
Accepted 3 June 2013
Available online 13 June 2013

Keywords:
Rate model
Anion exchange chromatography
Mass transfer
Parameter estimation
Big beads

ABSTRACT

This work presents a systematic procedure for using the general rate model to predict experimental chromatograms. The model considered axial dispersion, interfacial film mass transfer and intraparticle diffusion with parameters that have been intensively investigated in classical chemical engineering mass-transfer research. Theoretical equations, mass-transfer correlations and experimental procedures for obtaining bed voidage, particle porosity, mass-transfer parameters and Langmuir isotherm parameters are described. Three simple experiments were used to obtain system delay volume, bed voidage and particle porosity, respectively. Mass-transfer parameters were estimated using existing correlations in the literature without the need for additional experiments. A complete example was used to illustrate the approach. The model satisfactorily predicted the partial breakthrough curve of bovine serum albumin on a chromatography column packed with large anion-exchange particles with a nominal diameter of 90 μm. A parameter sensitivity analysis indicated the importance of accurate intraparticle diffusion modeling and demonstrated that lumped-particle models would be inadequate for understanding chromatographic behavior of large particles.

© 2013 Elsevier B.V. All rights reserved.

1. Introduction

Liquid chromatography (LC) modeling can be very helpful in the design of various LC packing media and LC processes. A typical LC model has two major components. One is the mass transfer and the other a binding mechanism. Various types of models for LC exist for the modeling and scale-up of different modes of LC [1]. They include the local equilibrium model [2], the plate model [3], the stochastic–dispersive model [4], the lumped-particle model [5,6], the pore diffusion model [7,8] and the general rate model [1,9–11]. Lee et al. reviewed different rate expressions for the particle phase in LC models [12].

The general rate model for LC considers axial dispersion, interfacial film mass transfer between the bulk-fluid and the particles in a packed bed, and intraparticle diffusion [10]. An adsorption isotherm or a reaction kinetic expression such as the second-order kinetics for affinity LC [13,14] is needed by the particle-phase mass transfer balance equation. Although early researchers considered the general rate model too complicated for LC modeling and difficult to solve numerically [6] on slow personal computers (PCs) in the 1980s, they have many unsurpassed advantages. The numerical difficulty in solving the general rate model is no longer a concern nowadays due to fast PCs. With efficient numerical methods such as the finite element method and the orthogonal collocation method, computation times on Pentium IV 3-GHz PCs are usually a matter of seconds or much less. Thus, there is no longer a need for model simplification for the sake of an easier numerical solution. The three mass transfer mechanisms in the general rate model are classical chemical engineering approaches to mass transfer in packed beds (also known as fixed-beds) that include LC columns. They have been intensively investigated over the years, especially in fixed-bed adsorption [15], resulting in numerous theoretical and empirical relationships for use in LC modeling. The coefficients for the three mass transfer mechanisms can be readily obtained from existing correlations in the literature without costly experiments. They also have surprisingly good accuracies. For example, in the absence of a binding mechanism, Li et al. [16] found that their general rate model for Size Exclusion Chromatography (SEC) predicted experimental chromatograms in preparative SEC separation of myoglobin and ovalbumin extremely well. In affinity LC with a second-order kinetics for binding, Gu et al. [14] showed that their general rate model for affinity LC predicted protein loading and elution very well.

In reality, the Biot number for mass transfer in an LC column that is the characteristic ratio of film mass transfer to intraparticle

* Corresponding author. Tel.: +1 740 593 1499; fax: +1 740 593 0873.
E-mail address: gu@ohio.edu (T. Gu).

1383-5866/$ - see front matter © 2013 Elsevier B.V. All rights reserved.
http://dx.doi.org/10.1016/j.seppur.2013.06.004

Nomenclature

A_1	area above a breakthrough curve (time · concentration)
A_2	area under a breakthrough curve (time · concentration)
a	Langmuir isotherm parameter (dimensionless), bC^{∞}
b	Langmuir isotherm parameter (mol^{-1} L)
Bi	Biot number for mass transfer, $kR_p/(\varepsilon_p D_p)$
C_0	feed concentration of a solute, max $\{C_f(t)\}$ (mol L^{-1})
C_b	concentration of a solute in the bulk-fluid phase (mol L^{-1})
c_b	C_b/C_0
C_p	concentration of a solute in the stagnant-fluid phase inside particle macropores (mol L^{-1})
c_p	C_p/C_0
C^{∞}	adsorption saturation capacity based on unit volume of particle skeleton (mol L^{-1})
C_p^*	concentration of a solute in the stationary phase based on unit volume of particle skeleton (mol L^{-1})
c_p^*	C_p^*/C_0
CA	dimensionless column holdup area for a breakthrough curve
d_m	molecular diameter (Å)
d_c	column inner diameter (cm)
d_p	average particle macropore diameter (Å)
D_b	axial dispersion coefficient (cm^2 s^{-1})
D_m	molecular coefficient (cm^2 s^{-1})
D_p	effective diffusivity in particle macropores (cm^2 s^{-1})
k	interfacial film mass-transfer coefficient (cm s^{-1})
L	column length (cm)
N	number of interior collocation points
N_e	number of quadratic finite elements
N_s	number of components
Pe_L	Peclet number of axial dispersion for a solute, vL/D_b
Q	mobile phase flow rate (ml s^{-1}), $\pi d_c^2(v\varepsilon_b)/4$
Q_s	Static binding capacity of BSA (mg/ml resin)
R	radial coordinate for a particle in spherical coordinate system
R_p	particle radius (cm)
Re	Reynolds number for packed-bed column (dimensionless), $(2R_p)v\varepsilon_b\rho/\mu$
Re′	modified Reynolds number, $Re/(1-\varepsilon_b)$
r	dimensionless radial coordinate, R/R_p
t	dimensional time (s), $\tau(L/v)$
t_e	time point on a breakthrough curve when the concentration has leveled off (s)
v	interstitial velocity (cm s^{-1})
V_b	column packed-bed volume (ml)
Z	column axial coordinate in cylindrical coordinate system
z	dimensionless column axial coordinate in cylindrical coordinate system, Z/L

Greek letters

ε_b	bed voidage or bed void fraction (dimensionless)
ε_p	particle porosity (dimensionless)
ξ	dimensionless mass-transfer parameter, $3Bi\cdot\eta(1-\varepsilon_b)/\varepsilon_b$
η	dimensionless mass-transfer parameter, $\varepsilon_p D_p L/(R_p^2 v)$
μ	mobile phase viscosity (Pa s)
ρ	mobile phase liquid density (kg/m^3)
τ	dimensionless time, vt/L
τ_{tor}	particle tortuosity (dimensionless)

diffusion is often far greater than 2. This means intraparticle diffusion dominates. Thus, lumped particle models are inadequate for some LC modeling situations, especially for large particles ("big beads") that have diameters reaching around 100 μm or higher instead of 10 or 20 μm.

Breakthrough of a protein from an adsorption LC column during the loading step of an LC process is closely monitored in process-scale LC to determine the time to terminate the step. Sometimes, a partial breakthrough curve at 10% of the UV reading of the complete breakthrough is used as a measure to terminate the loading step in order to save the feed. Also, in cases where the feed protein concentration is very low it can take extremely long time to obtain a complete breakthrough curve. In the above situations partial breakthrough curves are desired in practice.

In this work, the general rate model with Langmuir isotherm was used to predict the experimental partial breakthrough curve for Bovine Serum Albumin (BSA) on a column packed with 90 μm beads. A systematic procedure to measure and calculate various parameters in the model was presented in detail. The online supplementary material to this work contains a spreadsheet for calculating the parameters. The PC-based software program with a graphical user interface used in this work is available upon request at no cost for academic uses, making all the simulation results in this work readily reproducible by others.

2. Theory

2.1. Rate model equations

The general rate model for multicomponent LC consists of the following two partial differential equations [10],

$$-D_{bi}\frac{\partial^2 C_{bi}}{\partial Z^2}+v\frac{\partial C_{bi}}{\partial Z}+\frac{\partial C_{bi}}{\partial t}+\frac{3k_i(1-\varepsilon_b)}{\varepsilon_b R_p}(C_{bi}-C_{pi,R=Rp})=0 \quad (1)$$

$$(1-\varepsilon_p)\frac{\partial C_{pi}^*}{\partial t}+\varepsilon_p\frac{\partial C_{pi}}{\partial t}-\varepsilon_p D_{pi}\frac{1}{R^2}\frac{\partial}{\partial R}\left(R^2\frac{\partial C_{pi}}{\partial R}\right)=0 \quad (2)$$

The following multicomponent Langmuir isotherm is used for adsorption LC,

$$C_{pi}^*=\frac{a_i C_{pi}}{1+\sum_{j=1}^{N_s} b_j C_{pj}} \quad (3)$$

Other nonlinear multicomponent isotherms can also be used. The three equations above can be nondimensionalized as follows,

$$-\frac{1}{Pe_{Li}}\frac{\partial^2 c_{bi}}{\partial z^2}+\frac{\partial c_{bi}}{\partial z}+\frac{\partial c_{bi}}{\partial \tau}+\xi_i(c_{bi}-c_{pi,r=1})=0 \quad (4)$$

$$(1-\varepsilon_p)\frac{\partial}{\partial \tau}c_{pi}^*+\varepsilon_p\frac{\partial c_{pi}}{\partial \tau}-\eta_i\frac{1}{r^2}\frac{\partial}{\partial r}\left(r^2\frac{\partial c_{pi}}{\partial r}\right)=0 \quad (5)$$

$$c_{pi}^*=\frac{a_i c_{pi}}{1+\sum_{j=1}^{N_s}(b_j C_{0j})c_{pj}} \quad (6)$$

The nonlinear dimensionless Partial Differential Equation (PDE) system consisting of Eqs. (4) and (5) requires the following initial and boundary conditions:

Initial conditions: At $\tau = 0$, $c_{bi} = c_{bi}(0,z) = 0$, $c_{pi} = c_{pi}(0,r,z) = 0$.

Boundary conditions:

At $z = 0$,

$$\partial c_{bi}/\partial z = \mathrm{Pe}_{Li}[c_{bi} - C_{fi}(\tau)/C_{0i}] \quad (7)$$

and at $z = 1$,

$$\partial c_{bi}/\partial z = 0. \quad (8)$$

At $r = 0$,

$$\partial c_{pi}/\partial r = 0 \quad (9)$$

and at $r = 1$,

$$\partial c_{pi}/\partial r = \mathrm{Bi}_i(c_{bi} - c_{pi,r=1}) \quad (10)$$

The dimensionless feed concentration at the column inlet $C_{fi}(\tau)/C_0$ is fixed at unity for breakthrough analysis. For elution, $C_{fi}(\tau)/C_0$ is unity for $0 \leqslant \tau \leqslant \tau_{imp}$ and $C_{fi}(\tau)/C_0$ is set to zero for $\tau > \tau_{imp}$, where τ_{imp} is the dimensionless time duration for a rectangular pulse feed with a feed concentration of C_0.

The model system has been solved numerically using the finite element method for the discretization of z and the orthogonal collocation method for r [17]. Because this work modeled only a single-component BSA system, mg/ml can be used for concentrations instead of using mol/L. For multicomponent systems, molar concentration is preferred so the thermodynamic consistency of the multicomponent Langmuir isotherm (i.e., equal molar saturation capacities for all binding species) can be readily assessed [15]. For this work, the following parameters had to be obtained before simulation: $\mathrm{Pe_L}$, η, Bi, a, b, ε_a, and ε_p. Other parameters such as flow rate, column dimensions, particle diameter and particle macropore diameter were readily available.

2.2. Parameter estimation

Bed voidage (ε_b) and particle porosity (ε_p) are two important parameters in the general rate model. They are physical properties related to the bed and particle structures. They can be obtained experimentally using breakthrough curves for a blue dextran solution and a solvent (or salt) solution. Blue dextran is a polymer with a very large molecular weight. It does not penetrate particle macropores, while a solvent such as acetone penetrates the macropores.

Fig. 1 shows a schematic diagram of a breakthrough curve. For a column that does not retain the solute anywhere inside the column (i.e., zero column volume), the breakthrough curve should be a straight vertical line at time zero. However, the breakthrough curve of a solute is always delayed by a column. The delay is attributed to the following factors: solute retained in the fluid in the void space surrounding particles, solute in the fluid in the particle macropores and solute adsorbed on the stationary-phase particles. A simple mass balance in Fig. 1 for the solute in a single-component system that penetrates particle macropores and binds with the particles with the Langmuir isotherm behavior yields,

$$QC_0t_e = \left[V_b\varepsilon_bC_0 + V_b(1-\varepsilon_b)\varepsilon_pC_0 + V_b(1-\varepsilon_b)(1-\varepsilon_p)\frac{aC_0}{1+bC_0}\right] + QA_2 \quad (11)$$

For a non-binding blue dextran breakthrough curve, the equation above becomes,

$$QC_0t_e = V_b\varepsilon_bC_0 + QA_2 = V_b\varepsilon_bC_0 + Q(C_0t_e - A_1) \quad (12)$$

which yields the equation below that can be used to obtain ε_b based on the column holdup capacity area A_1 in Fig. 1,

$$\varepsilon_b = QA_1/(V_bC_0) \quad (13)$$

For a non-binding small solute such as acetone in a breakthrough analysis, Eq. (11) reduces to,

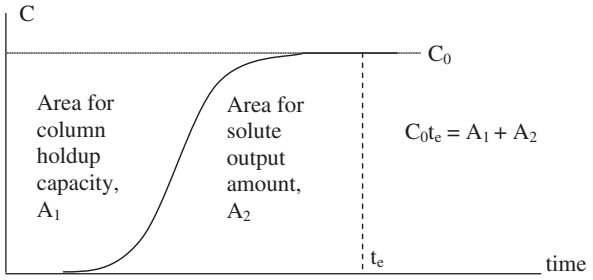

Fig. 1. Schematic diagram of the breakthrough curve of a single-component system.

$$QC_0t_e = V_b\varepsilon_bC_0 + V_b(1-\varepsilon_b)\varepsilon_pC_0 + Q(C_0t_e - A_1) \quad (14)$$

which yields,

$$A_1Q/(C_0V_b) = \varepsilon_b + (1-\varepsilon_b)\varepsilon_p \quad (15)$$

Inserting the following expression into Eq. (15)

$$Q = \pi d_c^2(v\varepsilon_b)/4 = (V_b/L)(v\varepsilon_b) = (v/L)V_b\varepsilon_b \quad (16)$$

gives,

$$[A_1 v/(LC_0)]\varepsilon_b = \varepsilon_b + (1-\varepsilon_b)\varepsilon_p \quad (17)$$

Eq. (17) is equivalent to the following nondimensionalized equation that can be used to obtain ε_p,

$$CA \cdot \varepsilon_b = \varepsilon_b + (1-\varepsilon_b)\varepsilon_p \quad (18)$$

where CA is the dimensionless column holdup capacity, or area A_1 in Fig. 1 nondimensionalized by dividing it by the dimensionless time conversion factor L/v and the breakthrough level-off concentration C_0.

Similarly, the following equation can be obtained by not dropping the isotherm term in Eq. (11) during the derivations for Eq. (18) or a solute that binds with the stationary phase,

$$CA \cdot \varepsilon_b = \varepsilon_b + (1-\varepsilon_b)\varepsilon_p + (1-\varepsilon_b)(1-\varepsilon_p)\frac{a}{1+bC_0} \quad (19)$$

with ε_b and ε_p known, Eq. (19) can be used to obtain Langmuir isotherm parameters a and b for a single-component with a minimum of two experimental breakthrough curves at two different C_0 values. If more than two C_0 values are available, Eq. (19) can be readily linearized for linear regression of a and b values. This kind of breakthrough analysis for isotherm parameters may require a large amount of solute if the column is not very small. As an alternative, the batch adsorption method can be used. A double reciprocal linear plot of $1/C_p$ vs. $1/C_p^*$ derived from the Langmuir isotherm can be used for data regression,

$$\frac{1}{C_p^*} = \frac{1}{a}\cdot\frac{1}{C_p} + \frac{b}{a} \quad (20)$$

The ε_b, ε_p, a and b values obtained from a small column may be used for the prediction of a larger column for scale-up. It is assumed that the columns have similar packed bed densities. A high column pressure may compress the packed bed if the packing material is not rigid enough such as in the case of soft gel beads. This will cause all these values to differ significantly.

2.3. Correlations for mass-transfer parameter estimation

The rate model requires three dimensionless mass-transfer parameters. They are Pe, η and Bi numbers. Their values depend on individual mass-transfer parameters such as axial dispersion coefficient (D_b), interfacial film mass-transfer coefficient (k) and intraparticle diffusivity (D_p). Unfortunately, it is not necessary to obtain these mass-transfer parameters experimentally, which can

be costly and often not easy because the three parameters are mingled together contributing to the shapes of simulated chromatograms, which makes experimental determination of individual mass-transfer parameters inaccurate. Various correlations are available for their estimation, thanks to the intensive studies in classical chemical engineering mass-transfer research.

2.3.1. Pelect number estimation

The axial Peclet number (Pe_L) depends on v, L and D_b. There are two primary mechanisms that contribute to axial dispersion in a fixed bed. One is molecular diffusion and the other turbulent mixing due to splitting and merging of flows around the particles [15]. The axial dispersion coefficient (D_b) may be estimated using a semi-empirical correlation obtained by de Ligny [18] for liquid flow in packed beds with spherical particles,

$$D_b = 0.7D_m + \frac{5.0R_p v}{1 + 4.4D_m/(R_p v)} \tag{21a}$$

in which the first term (molecular diffusion) on the right hand side comes from Langer at al. [19] and second from Giddings' random-walk analysis [20]. The molecular diffusivity (D_m) can be estimated based on the solute's molecular weight (MW) using the following correlation from Polson [21],

$$D_m(\mathrm{cm}^2/\mathrm{s}) = 2.74 \times 10^{-5}(\mathrm{MW})^{-1/3} \tag{22}$$

Another correlation for Pe_L is the popular Chung and Wen empirical correlation [22],

$$D_b = \frac{2R_p v\varepsilon_b}{0.2 + 0.011\mathrm{Re}^{0.48}} \quad (10^{-3} < \mathrm{Re} < 10^3) \tag{23a}$$

which is independent of D_m. The Reynolds number in mass transfer correlations often uses the superficial velocity (i.e., "empty-tower" velocity or $v\varepsilon_b$) instead of the interstitial velocity v (i.e., "fluid velocity"). The Reynolds number in LC is usually much smaller than 1. Thus, Eq. (23a) simplifies to,

$$D_b \approx 10R_p v\varepsilon_b \quad (10^{-3} < \mathrm{Re} < 1) \tag{23b}$$

This approximate relationship suggests that axial dispersion is directly proportional to interstitial velocity (v) for a given packed bed. Chung and Wen [22] suggested that D_b/D_m is often above 10^1 or 10^2. Thus, they ignored the molecular diffusion contribution to axial dispersion. For very small D_m (i.e., the solute has a very large MW), Eq. (21a) reduces to Eq. (21b),

$$D_b \approx 5.0R_p v \tag{21b}$$

It will result in the same D_b and Pe_L values as Eq. (23b) for a packed bed with $\varepsilon_b = 0.5$. For other ε_b values, the Pe_L value calculated from the de Ligny correlation deviates from that calculated using the simplified Chung and Wen correlation considerably. The Chun and Wen correlation is more robust because it is based on a large amount of experimental data for packed beds. Thus, the de Ligny correlation should not be used for these ε_b values. A modified de Ligny correlation is hereby introduced to incorporate the bed voidage for use in LC simulation,

$$D_b = 0.7D_m + \frac{10R_p v\varepsilon_b}{1 + 2.2D_m/(R_p v\varepsilon_b)} \quad (\mathrm{Re} < 1) \tag{21c}$$

This new correlation containing the bed voidage agrees surprisingly well with the simplified Chung and Wen correlation, i.e., Eq. (23a), for almost any reasonable ε_b values while it is still able to account for the small variations caused by a very wide range of D_m values. It can be particularly useful for slow-flow columns packed with small particles, resulting in a significant molecular diffusion contribution to D_b, especially for small solute molecules.

There are much more data on gas flow than liquid flow in packed beds. Axial dispersion behaviors differ considerably for these two types of flow [15]. Correlations for D_b and Pe_L are mostly based on larger particles than those used in LC [22] causing possible errors. Fortunately, in practice, for LC simulation cases in which the chromatograms are not very diffused (usually with fairly large Pe_L), their simulation can be rather insensitive to Pe_L variations. Thus, Pe_L estimation does not have to be stringent in these cases. If needed, a parameter sensitivity analysis can always be used for verification.

2.3.2. η Number estimation

The effective intraparticle diffusivity (D_p) is needed to calculate the dimensionless number defined as $\varepsilon_p D_p L/(R_p^2 v)$ by Gu et al. [10]. D_p can be obtained from the following experimental correlation [23],

$$D_p = D_m\left[1 - 2.104(d_m/d_p) + 2.09(d_m/d_p)^3 - 0.95(d_m/d_p)^5\right]/\tau_{tor} \tag{24}$$

The tortuosity τ_{tor} value usually falls in the range of 1.5 to over 10 and a reasonable value for many commercial porous solids is around 2–6 [24,25]. The τ_{tor} value is almost always unavailable from LC separation media vendors and it is not easily measured experimentally. It may be used as an adjustable parameter for curve fitting. In this work, τ_{tor} was set to a value of 4 (average of 2 and 6) for simulation. In Eq. (24), the average particle macropore diameter (d_p) is often available from vendors. For spherical molecules, the molecular diameter d_m can be calculated based on the solute's molecular weight from the following semi-empirical correlation for proteins in water according to Gu et al. [26],

$$D_m\ (\text{Å}) = 1.44(\mathrm{MW})^{1/3} \tag{25}$$

2.3.3. Biot number estimation

To obtain the Biot number for mass transfer (Bi) defined as $kR_p/(\varepsilon_p D_p)$, the following Wilson and Geankoplis empirical correlation can be used to calculate the film mass transfer coefficient (k) [27] first,

$$k = 0.687v^{1/3}(\varepsilon_b R_p/D_m)^{-2/3} \quad (0.0016 \leqslant \mathrm{Re} \leqslant 55) \tag{26}$$

in which 0.687 is a dimensionless coefficient. Another popular empirical correlation for k is from Kataoka et al. [28] with a dimensionless coefficient of 1.165,

$$k = 1.165v^{1/3}(R_p/D_m)^{-2/3}[(1-\varepsilon_b)/\varepsilon_b]^{1/3} \quad (\mathrm{Re}' < 100) \tag{27}$$

The ratio of the two k values calculated using Eqs. (26) and (27) is $0.590/[\varepsilon_b(1-\varepsilon_b)]^{1/3}$ [26], which deviates only 6% or less from unity for $0.25 < \varepsilon_b < 0.75$. It is remarkable that Kataoka et al. used more sets of experimental data and still got a correlation that yields similar values as Wilson and Geankoplis correlation. The very good agreement between the two correlations provides confidence on the accuracy of these two correlations. Kataoka et al. [28] also showed that the Carberry empirical correlation [29] deviated significantly from experimental data for $\mathrm{Re}' < 10$ (common for LC operations). Thus, it is not recommended for LC. The Pfeffer correlation [30] agrees with the correlation of Kataoka et al. much better with a slightly larger Sherwood number value (leading to a lager k value) consistently as demonstrated by Kataoka et al. [28]. However, the Pfeffer correlation is inconvenient to use due to its assumption of an outer fluid envelope covering an inner particle.

Luckily, the argument over which correlation to use for k is often moot. In LC modeling, the small difference in k typically produces no practical difference in simulated chromatograms. The simulated chromatograms are rather insensitive to a small Bi

variation due to variation in k when the Bi number is quite large already (i.e., well within intraparticle diffusion control already). In this work, the Wilson and Geankoplis correlation was adopted without prejudice against the correlation of Kataoka et al. If desired, a breakthrough curve for a protein may be used for curve-fitting to obtain one of its mass transfer parameters for comparison with the value obtained from a correlation.

3. Experimental

3.1. Materials

Anion exchange (AEX) LC beads (Q Sepharose® Fast Flow) of 90 μm nominal diameter were obtained from GE Healthcare Bio-Sciences Corporation (Piscataway, NJ). The average particle macropore diameter (d_p) for the beads is 300 Å. Buffers for LC experiments were prepared using deionized water from a MilliQ® water purification system and filtered using a 0.2 μm Stericup® filters (EMD Millipore, Bedford, MA) prior to use. Blue dextran (Cat. No. D5751) for ε_b measurement, acetone (Cat. No. 650501) for ε_p measurement, and BSA (Cat. No. A7906) for breakthrough analysis were obtained from Sigma–Aldrich (St. Louis, MO).

3.2. Static binding experiment for isotherm determination

The adsorption isotherm of BSA on the AEX beads was determined using a standard batch adsorption procedure. The 90 μm beads were packed in a drippy column under a suction vacuum of less than 5 psi accompanied by tapping the column to obtain a well consolidated bed with 1 ml bed volume. The beads were resuspended in 4 ml of Tris buffer (50 mM, pH 8), of which 0.5 ml was added to 14 ml of BSA solution of a certain concentration. The suspension was allowed to mix on a shaker for 6 h at room temperature, following which the beads were allowed to settle by gravity and the concentration of the supernatant was measured at a UV wavelength of 280 nm. The difference between the initial and final solution concentration was normalized to the resin volume (0.1 ml) to obtain the static binding capacity (Q_s, same as C_p^*) at the respective BSA concentration. Finally the equilibrium solution concentration was plotted against Q_s to obtain the adsorption isotherm.

3.3. Breakthrough experiment

The 90 μm beads were flow packed as per manufacturer's recommendation into a glass column (Omnifit®, Fischer Scientific, Pittsburg, PA) with a 0.66 cm inner diameter and a bed height of 7 cm to give a total volume of 2.39 ml. To ensure that the column was properly packed, it was qualified by measuring Height Equivalent of a Theoretical Plate (HETP) and asymmetry using an acetone pulse method prior to use [31]. The breakthrough experiment was performed using a BioCAD FPLC system (Applied Biosystems, now Life Technologies Corporation, Bedford, MA). The void volume of the column was measured from the complete breakthrough curve of 3 mg/ml blue dextran prepared in 50 mM sodium phosphate buffer with 2 M NaCl at a flow rate of 0.488 ml/min and a UV wavelength of 280 nm. NaCl was added to minimize binding of blue dextran to the positively charged anion exchange media. Similarly, the complete breakthrough curve of 5% (v/v) acetone in water was used to determine ε_p of the beads in the column at a flow rate of 0.488 ml/min and a UV wavelength of 254 nm. A partial BSA breakthrough curve with a BSA feed concentration of 0.25 mg/ml in 50 mM Tris at pH 8 was measured at a flow rate of 0.244 ml/min and a UV wavelength of 280 nm. This partial breakthrough curve was used to compare with model prediction as an example.

4. Results and discussion

4.1. Parameter estimation

4.1.1. System delay time

For simplicity in model presentation, the generate rate model always assumes time zero is the time when the solute first enters the inlet of the column. It also assumes that the effluent exits the column and is detected by a detector right away without any delay. In essence, both pre-column delay and post-column delay are set to zero in modeling. This means that if a column has a zero packing volume, the chromatogram should have a zero retention time if a pulse exits a sample injector. In LC modeling, the pre- and post-column delays may be negligible if the delays are due to tubing volumes that are very small compared with the column volume.

For low-pressure systems with small column volumes, long and large diameter plastic tubing can cause a significant delay of solute entering the column if the column volume is not very large. A longer delay is possible if a mobile phase reservoir containing a solute is switched to a different reservoir for breakthrough analysis. Both pre- and post-column delays cause a shift of time scale in an experimental chromatogram. In order to match a simulated chromatogram with an experimental chromatogram, the combined delays should be subtracted from the time axis of the experimental chromatogram before comparison.

Fig. 2 is the breakthrough curve of acetone obtained from switching from water to an acetone solution at time zero. The column had a bed volume of zero (i.e., the top plunger touched the column bottom intentionally). Diffusion was observed in the breakthrough curve because the curve was not straight up. The area above the curve was 135.7 (s · dimensionless concentration) after setting the y-axis at dimensionless concentration of unity at level-off based on linearity between absorbance and the relatively low acetone concentration. This meant that the system had a combined pre- and post-column delay time of 135.7 s or a system void volume of 1.104 ml based on the flow rate of 0.488 ml/min. This system void volume was significant compared with the column volume of 2.39 ml in the breakthrough tests below.

4.1.2. Bed voidage

Fig. 3 shows the raw data of blue dextran breakthrough on the 2.39 ml column with a flow rate of 0.488 ml/min. The area above

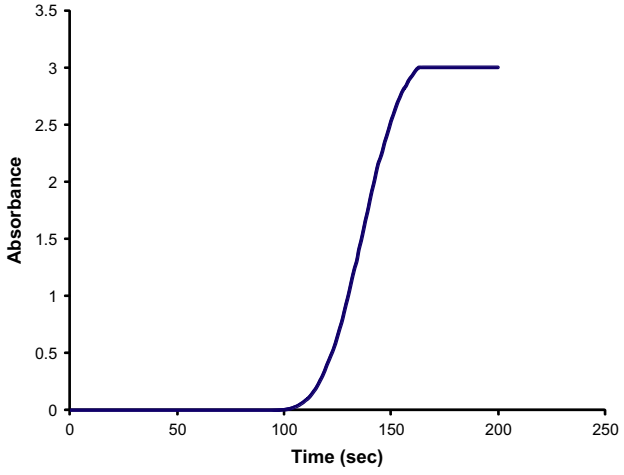

Fig. 2. Experimental acetone breakthrough curve on a column with zero bed volume for the measurement of the combined pre- and post-column delay time.

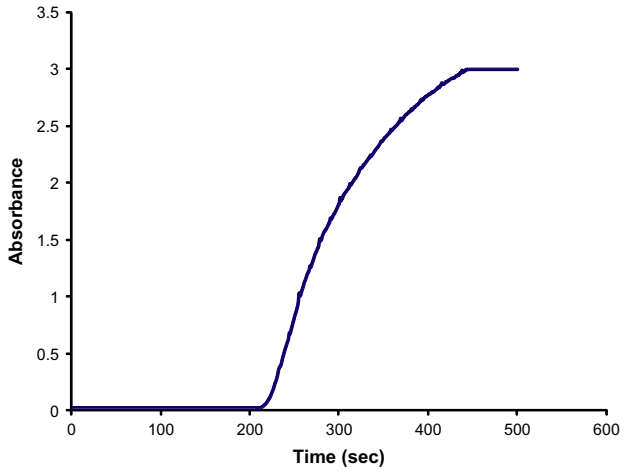

Fig. 3. Experimental blue dextran breakthrough curve.

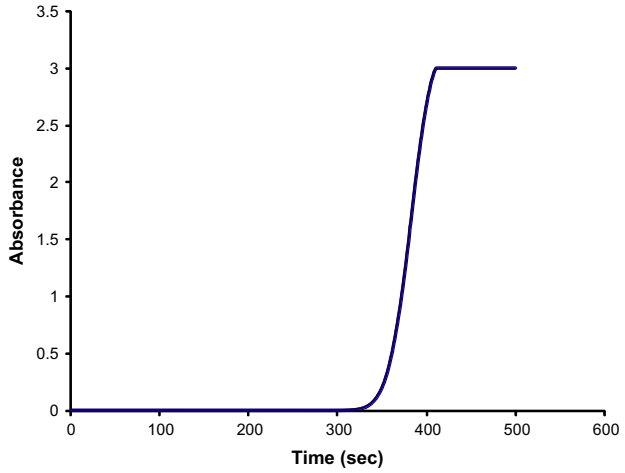

Fig. 4. Experimental acetone breakthrough curve.

the breakthrough curve (corresponding to A_1 in Fig. 1) was found to be 296.2 (s · dimensionless concentration) after shifting the baseline to zero and normalizing the breakthrough level-off Optical Density (OD) as dimensionless concentration 1. This value became A_1 = 160.5 (s · dimensionless concentration) after adjusting for the system delay time of 135.7 s. Plugging this value into Eq. (13) yielded the bed voidage ε_b = 0.545. With the bed voidage value known and a flow rate of 0.488 ml/min, the interstitial velocity was found to be v = 0.0436 cm/s according to Eq. (16).

4.1.3. Particle porosity

Fig. 4 shows the acetone breakthrough curve on the 2.39 ml column at a flow rate of 0.488 ml/min. It had a column hold-up capacity area of 378.0 (s · dimensionless concentration) from numerical integration of the breakthrough curve data. The area became 242.3 (s · dimensionless concentration) after adjusting for the system delay time. The dimensionless area above the acetone breakthrough curve was found to be CA = 1.51 by converting 242.3 using the L/v value of 160.5 s. Plugging the CA value into Eq. (18) yielded ε_p = 0.611.

4.1.4. Langmuir isotherm parameters

BSA adsorption on dextran based ion-exchange resins has been known to follow the Langmuir isotherm [32]. Fig. 5 shows the

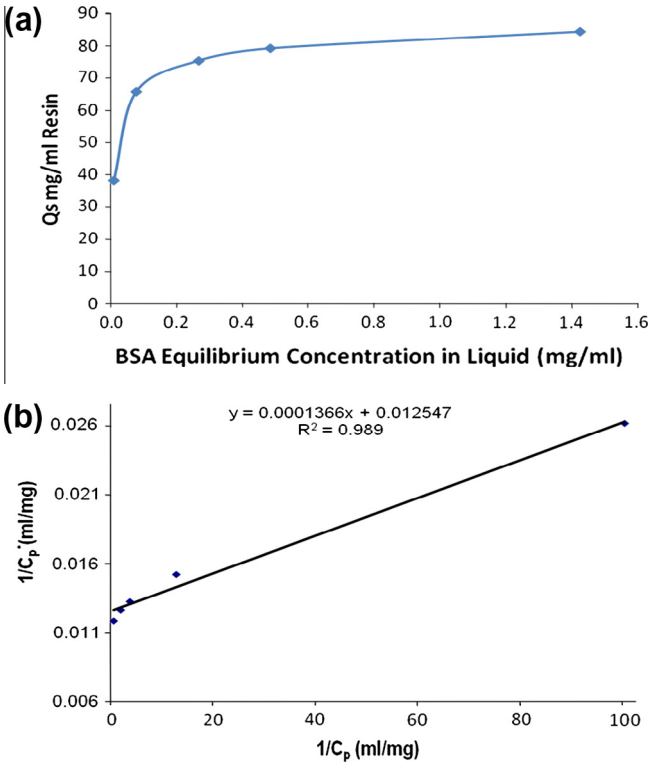

Fig. 5. Langmuir isotherm plots for BSA adsorption on 90 μm AEX beads.

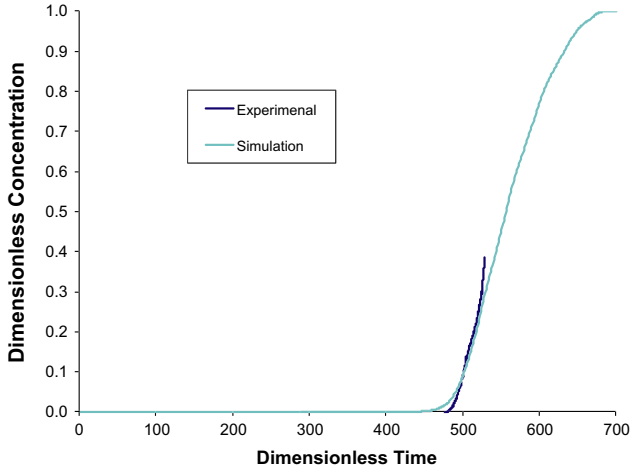

Fig. 6. Model prediction of BSA partial breakthrough curve (dimensionless time to dimensional time conversion factor L/v = 321 s).

batch adsorption isotherm of BSA on the AEX beads and the corresponding double reciprocal plot. The Langmuir isotherm parameter a was found to be 7321 (dimensionless) from the inverse of the slope. The y-intercept (b/a) was found to be 0.01255 ml/mg. Thus, the b was equal to 91.88 ml/mg. The stationary-phase BSA concentrations at equilibrium with different fluid-phase BSA concentrations were based on the unit volume of packed bed. This was incompatible with the rate model which requires the stationary-phase concentrations to be based on unit volume of particle skeleton. This means the a value should be divided by $(1-\varepsilon_b)(1-\varepsilon_p)$ before it could be used in the rate model. This had the same effect as dividing the C_p^* values by $(1-\varepsilon_b)(1-\varepsilon_p)$ for in y-axis in the double reciprocal plot. After this correction, a = 7321 became 41,363. If this often overlooked, yet very important, correction were not

Table 1
Parameters used for simulation software parameter input.[a]

Figure number	Dimensionless physical parameters							Numerical parameters	
	Pe_L	η	Bi	ε_b	ε_p	a	$b{\cdot}C_0$	N_e	N
6, 7, 8	285	0.99	58.6	0.545	0.611	41,363	91.88 × 0.25	30	6

[a] Pe_L = 285, 293, 320 calculated from Eqs. (23b), (21c), and (21a), respectively.

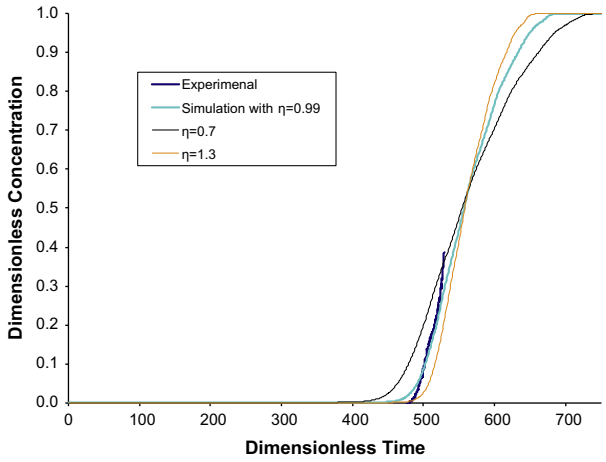

Fig. 7. Effect of dimensionless mass transfer parameter η on the simulated chromatogram.

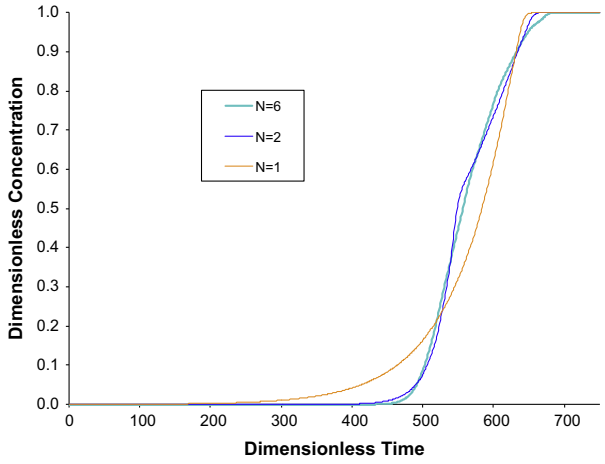

Fig. 8. Effect of the number of interior collocation points (N) for large particles.

made, the rate model would generate results with mass balance problems. If the breakthrough method with Eq. (19) is used to obtain a and b values, this correction is not required.

4.2. Simulation of BSA partial breakthrough

The general rate model was used to predict the partial breakthrough of BSA with a feed concentration of 0.25 mg/ml and a flow rate of 0.244 ml/min on the 2.39 ml column. The experimental partial breakthrough curve was adjusted for pre- and post-column delays due to a total system void volume of 1.104 ml. Because the packing material had a large saturation capacity (a/b) of 79.7 mg/ml, the breakthrough was greatly delayed (Fig. 6). Thus, in Fig. 6, the breakthrough curve started to take off at the dimensionless time of 480. This corresponds to a dimensional time of 42.8 h based on the column length of 7 cm and the interstitial velocity of 0.0218 cm/s (i.e., time conversion factor L/v = 321 s). This excessively long time was the reason why a small column was used in this work and also why the BSA breakthrough was terminated long before level-off. It should be pointed out that the diffused breakthrough curve in Fig. 2 was exaggerated due to the use of a very small time range (0–250 s) for plotting. If the time range in Fig. 2 is adjusted to cover the 0–40 h time range (in order to compare curve stiffness with Fig. 6), the breakthrough curve in Fig. 2 would appear extremely stiff without noticeable diffusion.

Fig. 6 shows that the model was able to predict the location and shape of the experimental curve satisfactorily. Parameters used for the simulation are listed in Table 1. Among the three dimensionless mass-transfer parameters (Pe_L, Bi and η only η had noticeable impact on the simulated breakthrough curve in this work. Adjusting Pe_L or Bi by ±30% would produce visually negligible difference in the simulated breakthrough curves. Fig. 7 shows the effect of adjusting the η value by ±30% on the simulated breakthrough curve. The η number is particular small for large particles with a large R_p value because η is inversely proportional to the R_p^2. A smaller η number would make the breakthrough curve more diffused (Fig. 7).

Fig. 8 shows that a large N value (the number of interior collocation points) should be used to describe the mass transfer inside the particle phase accurately. This is obviously because the column used in this work was packed with big beads. N = 1 was inaccurate as seen in Fig. 8. It corresponds to the use one exterior collocation point plus one built-in interior collocation point [17] to describe the concentration profile in a particle. The lumped particle approach uses only a single concentration point for the particle phase. Thus, this approach is even less accurate than the orthogonal collocation method with N = 1 for such big beads. Interestingly, Fig. 8 also shows that N = 2 produced a distortion (an inflexion point) in the middle of the breakthrough curve that was due to an inaccurate numerical method rather than the physical behavior of the system. This distortion would disappear when N = 3 was used. It was found that the simulated breakthrough curve hardly had any noticeable change for N = 3–6, indicating convergence.

5. Conclusions

This work used the general rate model to predict the partial breakthrough of BSA on a column packed with 90 μm Q Sepharose® Fast Flow AEX big beads satisfactorily with a systematic approach for parameter estimation. System delay volume, bed voidage and particle porosity were obtained from three simple experimental runs. The batch adsorption method was used to obtain Langmuir isotherm for BSA. It is noteworthy to stress that the units for the stationary-phase concentration should be based on particle skeleton volume rather than packed stationary-phase volume for the model. The Peclet number, the η number and the Biot number for mass transfer were all estimated using existing correlations without the need for any experiments. A parameter sensitivity analysis indicated that the η number had a large impact on the simulated breakthrough curve while the other two dimensionless numbers were insensitive for the studied case. This work

also indicated that for large particles, accurate modeling of the particle phase was necessary and lumped-particle models would be inadequate. The systematic approach in this work will help to propagate the use of the general rate model for LC modeling and scale-up.

Appendix A. Supplementary material

Supplementary data associated with this article can be found, in the online version, at http://dx.doi.org/10.1016/j.seppur.2013.06.004.

References

[1] Q. Yu, N.H.L. Wang, Computer simulations of the dynamics of multicomponent ion exchange and adsorption in fixed beds—gradient-directed moving finite element method, Comput. Chem. Eng. 13 (1989) 915–926.
[2] F.G. Helfferich, G. Klein, Multicomponent chromatography: theory of interference, M. Dekker, 1970.
[3] G. Guiochon, S. Ghodbane, Computer simulation of the separation of a two-component mixture in preparative-scale liquid chromatography, J. Phys. Chem. 92 (1988) 3682–3686.
[4] A. Felinger, A. Cavazzini, F. Dondi, Equivalence of the microscopic and macroscopic models of chromatography: stochastic–dispersive versus lumped kinetic model, J. Chromatogr. A 1043 (2004) 149–157.
[5] L. Lapidus, N.R. Amundson, A descriptive theory of leaching. Mathematics of adsorption beds, J. Phys. Chem. 56 (1952) 984–988.
[6] H. Moon, K.W. Lee, A lumped model for multicomponent adsorptions in fixed beds, Chem. Eng. Sci. 41 (1986) 1995–2004.
[7] L.E. Weaver, G. Carta, Protein adsorption on cation exchangers: comparison of macroporous and gel-composite media, Biotechnol. Progr. 12 (1996) 342–355.
[8] S. Zhang, Y. Sun, Study on protein adsorption kinetics to a dye–ligand adsorbent by the pore diffusion model, J. Chromatogr. A 964 (2002) 35–46.
[9] A.I. Liapis, R.J. Litchfield, Ternary adsorption in columns, Chem. Eng. Sci. 35 (1980) 2366–2369.
[10] T. Gu, G.J. Tsai, G.T. Tsao, New approach to a general nonlinear multicomponent chromatography model, AIChE J. 36 (1990) 784–788.
[11] T. Gu, G.J. Tsai, G.T. Tsao, Multicomponent affinity radial flow chromatography, Sep. Technol. 2 (1992) 176–182.
[12] W.C. Lee, S.H. Huang, G.T. Tsao, A unified approach for moments in chromatography, AIChE J. 34 (1988) 2083–2087.
[13] A.I. Liapis, Modelling affinity chromatography, Sep. Purif. Methods 19 (1990) 133–210.
[14] T. Gu, K.H. Hsu, M.J. Syu, Scale-up of affinity chromatography for purification of enzymes and other proteins, Enzyme Microbial Technol. 33 (2003) 430–437.
[15] D.M. Ruthven, Principles of Adsorption and Adsorption Processes, Wiley, New York, 1984.
[16] Z. Li, Y. Gu, T. Gu, Mathematical modeling and scale-up of size-exclusion chromatography, Biochem. Eng. J. 2 (1998) 145–155.
[17] T. Gu, Mathematical Modeling and Scale-Up of Liquid Chromatography, Springer, Berlin, New York, 1995.
[18] C.L. de Ligny, Coupling between diffusion and convection in radial dispersion of matter by fluid flow through packed beds, Chem. Eng. Sci. 25 (1970) 1177–1181.
[19] G. Langer, A. Roethe, K.P. Roethe, D. Gelbin, Heat and mass transfer in packed beds—III. Axial mass dispersion, Int. J. Heat Mass Transfer 21 (1978) 751–759.
[20] J.C. Giddings, Eddy diffusion in chromatography, Nature 184 (1959) 357–358.
[21] A. Polson, Some aspects of diffusion in solution and a definition of a colloidal particle, J. Phys. Chem. 54 (1950) 649–652.
[22] S.F. Chung, C.Y. Wen, Longitudinal dispersion of liquid flowing through fixed and fluidized beds, AIChE J. 14 (1968) 857–866.
[23] A. Striegel, W.W. Yau, J.J. Kirkland, D.D. Bly, Modern size-exclusion liquid chromatography: practice of gel permeation and gel filtration chromatography, Wiley, New York, 2009.
[24] C.J. Geankoplis, Drying of process materials, Transp. Process. Unit Oper. (1993) 520–583.
[25] C.N. Satterfield, Mass Transfer in Heterogeneous Catalysis, MIT Press, Cambridge, MA, 1970.
[26] T. Gu, Y. Zheng, A study of the scale-up of reversed-phase liquid chromatography, Sep. Purif. Technol. 15 (1999) 41–58.
[27] E.J. Wilson, C.J. Geankoplis, Liquid mass transfer at very low Reynolds Numbers in packed beds, Ind. Eng. Chem. Fund. 5 (1966) 9–14.
[28] T. Kataoka, H. Yoshida, K. Ueyama, Mass transfer in laminar region between liquid and packing material surface in the packed bed, J. Chem. Eng. Jpn. 5 (1972) 132–136.
[29] J.J. Carberry, A boundary-layer model of fluid-particle mass transfer in fixed beds, AIChE J. 6 (1960) 460–463.
[30] R. Pfeffer, Heat and mass transport in multiparticle systems, Ind. Eng. Chem. Fund. 3 (1964) 380–383.
[31] A.S. Rathore, R.M. Kennedy, J. O'Donnell, I. Bemberis, O. Kaltenbrunner, Qualification of a chromatographic column: why and how to do it, Biopharm. Int. 16 (2003) 30–40.
[32] H.S. Tsou, E.E. Graham, Prediction of adsorption and desorption of protein on dextran based ion-exchange resin, AIChE J. 31 (1985) 1959–1966.